Structure of incommensurate gold sulfide monolayer on Au(111)

Su Ying Quek[a)]
Division of Engineering and Applied Sciences, Harvard University, Cambridge, Massachusetts 02138-2902, USA

Monika M. Biener[b)]
Division of Engineering and Applied Sciences, Harvard University, Cambridge, Massachusetts 02138-2902, USA and Department of Chemistry and Chemical Biology, Harvard University, Cambridge, Massachusetts 02138-2902, USA

Juergen Biener[b)]
Center for Nanoscale Science, Harvard University, Cambridge, Massachusetts 02138-2902, USA

Joydeep Bhattacharjee[a)]
Theoretical Sciences Unit, Jawaharlal Nehru Centre for Advanced Scientific Research, Jakkur PO, Bangalore 560 064, India

Cynthia M. Friend
Division of Engineering and Applied Sciences, Harvard University, Cambridge, Massachusetts 02138-2902, USA and Department of Chemistry and Chemical Biology, Harvard University, Cambridge, Massachusetts 02138-2902, USA

Umesh V. Waghmare
Theoretical Sciences Unit, Jawaharlal Nehru Centre for Advanced Scientific Research, Jakkur PO, Bangalore 560 064, India

Efthimios Kaxiras[c)]
Division of Engineering and Applied Sciences, Harvard University, Cambridge, Massachusetts 02138-2902, USA and Department of Physics, Harvard University, Cambridge, Massachusetts 02138-2902, USA

(Received 6 October 2006; accepted 17 July 2007; published online 12 September 2007)

We develop an atomic-scale model for an ordered incommensurate gold sulfide (AuS) adlayer which has previously been demonstrated to exist on the Au(111) surface, following sulfur deposition and annealing to 450 K. Our model reproduces experimental scanning tunneling microscopy images. Using state-of-the-art Wannier-function-based techniques, we analyze the nature of bonding in this structure and provide an interpretation of the unusual stoichiometry of the gold sulfide layer. The proposed structure and its chemistry have implications for related S–Au interfaces, as in those involved in self-assembled monolayers of thiols on Au substrates. © *2007 American Institute of Physics*. [DOI: 10.1063/1.2770731]

I. INTRODUCTION

Nanostructured materials, such as two-dimensional confined systems, have attracted interest because their structural and electronic properties can differ substantially from those of bulk materials.[1,2] These systems are promising candidates for technological applications, including molecular electronic devices, sensors, and catalysts.[2–4] Advances in nanoscale growth methods have produced systems with interesting properties,[3–5] but better understanding of their atomistic-scale structure is often desired. In particular, incommensurate structures complicate theoretical analysis because the layer and substrate cannot both be treated exactly within a common unit cell.

In this work, we revisit the structure of an interesting incommensurate nanoscale system, the two-dimensional (2D) ordered layer of gold sulfide, formed on the Au(111) surface following sulfur deposition and annealing at 450 K.[5,6] This system can offer clues about the nature of possible precursor states for the bonding of organic molecules (such as alkylthiols) to Au via sulfur, which are of interest in technological applications.[3] The structure and chemistry of this gold sulfide layer are analyzed in detail within density functional theory by taking into account charge transfer in the incommensurate system and studying the nature of bonding using a recently developed Wannier-orbital-based technique. Our results are discussed in the context of the rich chemistry of Au and its compounds.[7,8]

[a)]Present address: The Molecular Foundry, Lawrence Berkeley National Laboratory, Berkeley, CA 94720.
[b)]Present address: Lawrence Livermore National Laboratory, 7000 East Ave., Livermore, CA 94550.
[c)]Author to whom correspondence should be addressed. Electronic mail: kaxiras@physics. harvard.edu

II. METHODS

The scanning tunneling microscopy (STM) experiments were performed in ultrahigh vacuum with a base pressure of 4×10^{-10} Torr. The Au(111) surface was cleaned by Ar^+ sputtering at 300 K, followed by annealing to 700 K for 10 min and 600 K for 60 min. The characteristic herringbone reconstruction was observed following this procedure. SO_2 (Matheson, anhydrous grade) was introduced by chamber backfilling. Only a small fraction of the SO_2 decomposes and deposits sulfur on the Au(111) surface, as monitored by Auger electron spectroscopy. No oxygen-containing species was detected on the surface at any time, suggesting that the oxygen released during SO_2 decomposition is removed by an abstraction reaction with excess SO_2.[9] Further experimental details can be found in Ref. 5.

All our calculations were performed in the framework of density functional theory with the generalized gradient approximation for the exchange-correlation functional (PW-91).[10] A plane-wave basis set was used, with scalar relativistic pseudopotentials to represent the atomic cores. All unit cells used in our calculations are within the experimental error bars of $(8.8\pm0.4)\times(8.2\pm0.4)$ Å^2. 4×4 and 8×8 k-point meshes per unit cell were used for calculations with and without the Au substrate, respectively. Typically, the total energy for structures we considered is well converged with a 3×3 k-point mesh per unit cell. At least 10 Å of vacuum was used in each calculation to separate the slab geometries, and convergence of relevant physical quantities was checked with respect to vacuum size. Within this framework, we introduced theoretical approaches to obtain, first, the atomic structure and, second, the bonding characteristics of the incommensurate AuS layer on Au(111).

In calculations for the atomic structure, we used the projected augmented wave method[11] with an energy cutoff of 280 eV, as implemented in VASP. The Au substrate was represented by a slab of six Au(111) layers, the bottom three of which are frozen in their bulk positions. Geometry optimization was performed with a force convergence criterion of 0.05 eV/Å. The resulting structures were used for analysis of bonding characteristics, by constructing localized Wannier functions from the Kohn-Sham wave functions. Further details of our theoretical approaches will be described below.

III. EXPERIMENTAL RESULTS

We have previously reported detailed scanning probe studies of the interaction of sulfur with Au(111).[5,6] These studies established that sulfur interacts with Au(111) in a dynamic, rather than static, manner, with large scale mass transport and the dislodgement of Au terrace atoms to form a gold sulfide phase. STM images[5] show that a sulfur coverage as low as 0.1 ML completely lifts the herringbone surface reconstruction of Au(111) even at room temperature (300 K). The presence of serrated step edges at these low coverages suggests that the released Au atoms are mobile and can attach to or leave the Au(111) step edges. At 0.3 ML, an ordered $(\sqrt{3}\times\sqrt{3})R30°$ adlayer of adsorbed sulfur atoms is formed. Above this coverage, a rearrangement of the Au surface atoms occurs, with small islands and monatomic etch pits nucleating on Au terraces, strongly suggesting that Au atoms are removed from terraces into a growing gold sulfide phase that is distinct from that of adsorbed sulfur observed at lower coverages. Similar incorporation of stoichiometric amounts of substrate atoms into adsorbate-induced surface adlayers has been observed in other systems, such as a 2D oxide layer on Pd(111) (Ref. 12) and a 2D sulfide on Al(111).[13] At a saturation coverage of 0.6 ML, the surface takes on a spongelike morphology that is completely covered by a 2D layer. Quasirectangular ringlike structures with some short-range order are formed when the system is subsequently annealed to 420 K. Similar features have been observed during the electrochemical deposition of S on Au;[14] it was proposed that these rings correspond to strained S_8 molecules. Further annealing to 450 K leads to Ostwald ripening of the original etch pits, resulting in large vacancy islands of monatomic depth. The S coverage drops to approximately 0.5 ML and a 2D layer with long-range order completely covers the Au surface. High-resolution STM images[5] of this ordered 2D phase reveal that the system is incommensurate, with a $(8.8\pm0.4)\times(8.2\pm0.4)$ Å^2 unit cell and an angle of $82°\pm4°$ between the lattice vectors. Based on the areas of the vacancy islands, it was estimated that approximately 0.5 ML of Au is incorporated into the ordered 2D sulfide layer, suggesting a 1:1 Au–S stoichiometry.[5] This stoichiometry is distinct from those of bulk gold sulfides, Au_2S and Au_2S_3.[15]

IV. ATOMIC STRUCTURE: APPROACH AND MODEL

The unusual stoichiometry and 2D nature of the gold sulfide layer suggest that it is a phase of unknown structure, distinct from three-dimensional bulk gold sulfides. The incommensurate nature implies that the AuS layer does not form strong directional bonds with the Au surface (this picture is later confirmed through our Wannier-orbital analysis of bonding in the proposed model structure). To construct an atomic-scale model, we consider the system in two stages. First, we determine the atomic structure of an isolated AuS layer in a fixed unit cell, consistent with experimental measurements, and in a fully relaxed cell. Next, we analyze how the substrate affects the atomic and electronic structures of this layer, taking into account the incommensurate nature of the interaction by averaging over several different configurations.

In the first step, given the Au(111) surface lattice, a reasonable starting point for the fixed unit cell is given by the black box in Fig. 1(a). This cell has a lattice constant of 8.65 Å (three times that of Au) in direction $\boldsymbol{a}_1$ and a lattice angle of 79°, both values within experimental error bars (8.65 Å is within the range of 8.4–9.2 Å for the first lattice constant). The lattice constant in direction $\boldsymbol{a}_2$ was fixed at the experimental value of 8.20 Å, which is not a simple multiple of the Au lattice constant. We considered several models with different numbers of atoms per unit cell, with stoichiometry Au:S=1:1, and different arrangements of these atoms, using information on the local coordination chemistry of Au and S in known compounds for guidance.[16,17] Fully relaxing the positions of these atoms within the fixed unit

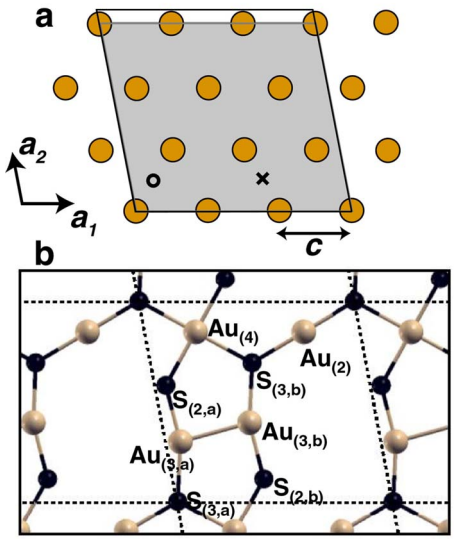

FIG. 1. (Color online) (a) Proposed orientation of AuS unit cell (black box). (b) Atomic structure of *A*. Numerical subscripts denote the coordination of each atom and letter subscripts indicate inequivalent atoms of the same coordination. The cross and circle in (a) (× and ○, respectively) are relevant to structure *B* described in the text.

cell resulted in only one stable structure (in all other structures, the atoms rearranged drastically and the atomic forces sometimes did not converge). The stable structure, which we call *A*, is planar with four Au and four S atoms per unit cell [Fig. 1(b)]. Details of bond lengths are given in Table I. The corresponding S coverage is 0.41 ML, assuming that a completely flat, unreconstructed Au(111) surface is entirely covered by the AuS layer. This coverage is close to the experimental estimate of 0.5 ML, taking into account the attachment of S atoms to the edges of Au vacancy islands present on the annealed, sulfide-covered Au(111) surface and the uncertainty in the experimental calibration.

We next allowed the unit cell parameters to relax without any constraints. This resulted in an almost uniform shrinking of the unit cell vectors. The lattice angle changed to 78° (which is within experimental error bars and close to the corresponding angle of 79° in structure *A*). The new lattice constants are 7.85 and 7.65 Å, which are, respectively, 9.3% and 6.7% smaller than the corresponding lattice constants in *A*. However, the ratio between lattice constants is 1.04, close to the corresponding ratio of 1.05 in *A*. The atomic geometry also remains very similar to that in *A* [Fig. 2(a)]. This shows that the atomic structure and unit cell shape in *A* are reasonable. The relaxed unit cell is too small compared to experimental values (the lower bound in experiment being 8.4 $\times$7.8 Å^2), but the shrinking of the unit cell upon relaxation is consistent with the shorter bond lengths found in bulk Au_2S (Ref. 16) and other compounds with Au–S bonds[17] (Table I). As discussed below, the larger unit cell observed in experiment may be stabilized by charge transfer from the Au substrate.

We now consider the effects of the Au substrate. First, we examine this effect on important structural features of the AuS monolayer. Although the combined system is incommensurate, it is possible to fit the AuS unit cell in a supercell of the Au(111) surface by using the equilibrium Au lattice constant predicted from calculations on bulk Au (c_{theor} =2.948 Å) instead of the experimental value (c_{expt} =2.884 Å). In this arrangement, the gray area in Fig. 1(a), which is commensurate with the Au lattice, has dimensions of 8.84$\times$7.80 Å^2, still within experimental error bars for the

TABLE I. Geometric features in structure *A*, in the fully relaxed neutral and charged (3.3*e* per cell) layers, and in experiment. $\boldsymbol{a}_1 \times \boldsymbol{a}_2$ and θ denote, respectively, the lattice dimensions (in Å) in the $\boldsymbol{a}_1$ and $\boldsymbol{a}_2$ directions and the angle between lattice vectors for the AuS unit cell. The remaining rows tabulate bond lengths (in Å) in the respective AuS models and in experiment. The experimental bond lengths are taken from the literature of known compounds that contain Au–S or Au–Au bonds with the same formal oxidation states as given in parentheses in the first column. Specifically, the bond length for Au^{I}–S^{-II} is taken from crystal data on bulk Au_2S (Ref. 16). In compounds with Au^{III}–S^{-II} bonds, typical Au^{III}–S^{-II} bond lengths are 2.40 Å if S bridges two Au^{III} atoms and 2.30–2.35 Å otherwise (Ref. 17). The Au^{II}–Au^{II} bond length is about 2.60 Å for covalent Au^{II}–Au^{II} bonds and 3.10 Å for weaker Au^{II}–Au^{II} aurophilic interactions (Ref. 17).

Geometric features	Structure *A*	Fully relaxed, neutral layer	Fully relaxed, charged layer	Experiment
$\boldsymbol{a}_1 \times \boldsymbol{a}_2$	8.7×8.2	7.9×7.7	8.4×7.9	(8.8±0.4)×(8.2±0.4)
θ (deg)	79	78	79	82±4
$Au_{(2)}$–$S_{(3)}$ (Au^{I}–S^{-II})	2.41	2.29	2.34	2.17[a]
$Au_{(3)}$–$S_{(2)}$ (Au^{II}–S^{-II})	2.33	2.25	2.30	···
$Au_{(3)}$–$S_{(3)}$ (Au^{II}–S^{-II})	2.41	2.28	2.35	···
$Au_{(4)}$–$S_{(2)}$ (Au^{III}–S^{-II})	2.45	2.37	2.42	2.30–2.35, 2.40[b]
$Au_{(4)}$–$S_{(3)}$ (Au^{III}–S^{-II})	2.58	2.37	2.43	2.30–2.35, 2.40[b]
$Au_{(3,a)}$–$Au_{(3,b)}$ (Au^{II}–Au^{II})	2.87	2.88	2.85	2.60, 3.10[b]

[a]Reference 16.
[b]Reference 17.

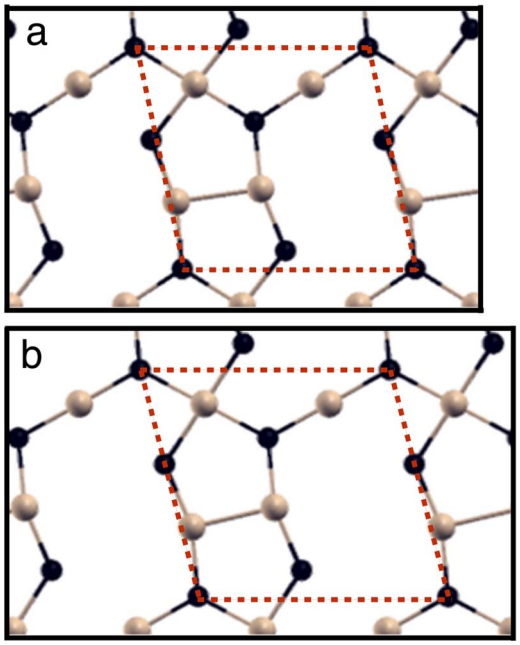

FIG. 2. (Color online) Fully relaxed structures and unit cells (red boxes) for isolated, (a) neutral and (b) charged AuS layers. The structure in (b) has a charge of 3.3*e* per cell.

AuS unit cell (7.80 Å is within the range of 7.8–8.6 Å for the second lattice constant). We can now perform geometry optimizations for a periodic system with a supercell containing a AuS layer on top of a six-layered Au(111) slab. In the most stable structure, which we call *B*, the twofold coordinated Au atom $[Au_{(2)}]$ in AuS is at site × and the fourfold coordinated Au atom $[Au_{(4)}]$ at site ○ (Fig. 1). Initial structures with $Au_{(2)}$ positioned at any of the threefold sites of the surface layer also relaxed to structure *B*. If $Au_{(4)}$ is placed initially at × and $Au_{(2)}$ at ○, each of these Au atoms remains at its initial site during geometry optimization and the remaining atoms completely rearrange to yield the same structure (*B*), with the Au atom at site × becoming twofold coordinated and that at ○ becoming fourfold coordinated. This indicates that the AuS layer in structure *B* is stable with respect to internal atomic rearrangements, when it is placed on the Au substrate.

The incommensurate nature and long-range order of the AuS layer imply that the layer should feel an average effect of the substrate which is not altered as the relative position of the overlayer is varied. The calculations mentioned so far cannot capture this effect because the forced matching of lattice constants between the overlayer and the substrate introduces artificial corrugations for some atomic positions. Therefore, in analyzing the electronic features of the AuS layer, it is necessary to introduce a different approach to take into account the average effects of the substrate on the incommensurate adlayer.

Since the overlayer and substrate do not form strong directional bonds with each other and are both metallic, charge transfer is expected to be the dominant electronic effect of the substrate (this assumption is confirmed by Wannier orbital analysis, as described later). This suggests that the AuS atomic geometry and electronic structure will remain largely unchanged by the Au substrate. Thus, in the following, we use the structural features of the stable isolated layer *A* and model charge transfer by changing the occupancy of the AuS states (so-called rigid band model). We model the change in occupancy by shifting the Fermi level (E_F) of *A* by an amount ΔE_F to that estimated for the combined system.

To estimate ΔE_F, we construct a series of models that are representative of the different relative positions that the incommensurate AuS layer can take on the Au(111) substrate. Next, we compute the average of the substrate-induced shifts in Fermi level at each of these positions. The models were constructed as follows. We first relax atoms in the top three Au(111) layers of the six-layer Au(111) slab and atoms in the AuS layer, with the additional constraint that the AuS layer be planar, with $Au_{(2)}$ at position × and $Au_{(4)}$ at position ○. The optimal height of the AuS layer above the Au surface is 2.53 Å, which is the same as the average height of the layer above the Au surface in structure *B*. We call the resulting system B'. We then shift this AuS layer in steps by $\lambda \boldsymbol{a}_2$ relative to the substrate ($\lambda = 0.0, 0.1, \ldots, 0.9$) resulting in systems which we call B'_λ [at each step, only the top three Au(111) layers are allowed to relax]. To find the substrate-induced shift in Fermi level ΔE_F, we take the average over λ of the differences in work functions $\Delta\Phi$ between the metallic systems *A* and B'_λ. The work functions of the systems are calculated using symmetric slabs, obtained by taking mirror images about the three frozen Au(111) layers, to give nine-layered Au slabs covered on both sides by AuS. The work function Φ is computed as $V^{(c)}_{\mathrm{vac}} - E^{(c)}_F$, where $E^{(c)}_F$ and $V^{(c)}_{\mathrm{vac}}$ are the Fermi level and vacuum potential in the calculation.

V. ATOMIC STRUCTURE: RESULTS

The energy difference between B'_λ and B' is typically 0.2–0.3 eV, except for $\lambda = 0.2$, 0.5, and 0.8, where the energy differences are 0.9, 0.6, and 0.9 eV, respectively. The average estimated E_F of the incommensurate AuS layer on Au(111) is 0.85 eV closer to the vacuum potential than E_F of *A*, corresponding to electronic charge transfer from Au(111) to *A*. The shifts in E_F calculated for each B'_λ range from 0.76 to 0.88 eV, with smaller shifts (less charge transfer) for the less stable B'_λ. The direction of charge transfer is consistent with the larger work function of *A* (6.18 eV) relative to Au(111), which we calculate to be 5.18 eV, in reasonable agreement with the experimental value[18] of 5.31 eV.

STM images are obtained from structure *A* with $\Delta E_F = 0.85$ eV using the Tersoff-Hamann approximation.[19] To take into account the effect of convolution between sample and tip wave functions,[19] as well as the small amount of spot broadening in the scan direction $\boldsymbol{x}$, we use elliptical Gaussian broadening with standard deviations s_x of 1.2 Å and s_y of 0.8 Å (both less than half of the bond lengths in the structure). Our simulations are in agreement with the high-magnification experimental images at two different sample bias voltages (Fig. 3) and are insensitive to the exact values of s_x and s_y.

In both images, the darkest portions correspond to the area between the eight-membered rings (no atoms), while the

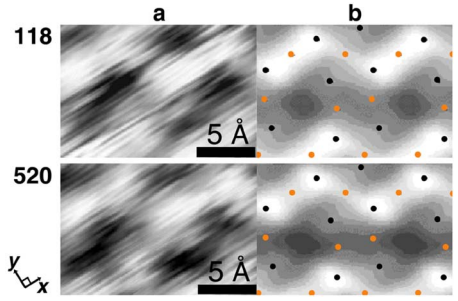

FIG. 3. (Color online) (a) Constant height STM images collected at room temperature, (b) STM simulations. Orange and black circles mark lateral positions of Au and S atoms, respectively. The numbers indicate sample bias voltages in mV, and the scan direction is given by $\boldsymbol{x}$.

bright spots are associated with positions of the $S_{(3,a)}$ and $S_{(3,b)}$ atoms. Atomic-orbital-projected densities of states (DOS) reveal that in the range 0.74–1.40 eV above E_F of the isolated layer A, the contribution to the DOS originates, in decreasing order, from $Au_4(5d)$, $S_{3,i}(3p)$, $S_{2,i}(3p)$, $Au_1(6s)$, and $Au_{3,i}(5d)$ $(i=a,b)$. The localized nature of Au d orbitals explains why $S_{3,i}(3p)$ are dominant in the images in Fig. 3, which probe the electronic states in the ranges (0.85–0.97) eV and (0.85–1.37) eV above E_F of A. Since the relative importance of the atomic-orbital contributions to the DOS does not change in the energy interval (0.74–1.40) eV above E_F of A, replacing ΔE_F by 0.78 or 0.88 eV (the extreme values of ΔE_F obtained in our calculations with B_λ') will not change the qualitative features of the simulated STM images. The energy windows relevant to these STM images are indicated by dashed lines in Fig. 4, which plots the atom-projected DOS. The plot indicates that the states probed by the two voltages are not very different, consistent with the similarity of the STM images at these voltages.

VI. NATURE OF BONDING: APPROACH

If Au atoms from terraces are indeed incorporated into a stable, incommensurate AuS layer, this calls for a more de-

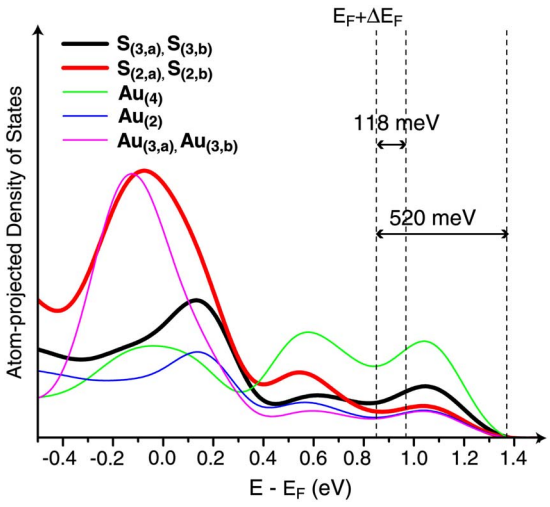

FIG. 4. (Color online) Atom-projected DOS (summed over orbitals) for structure A. E_F refers to the Fermi level of isolated layer A.

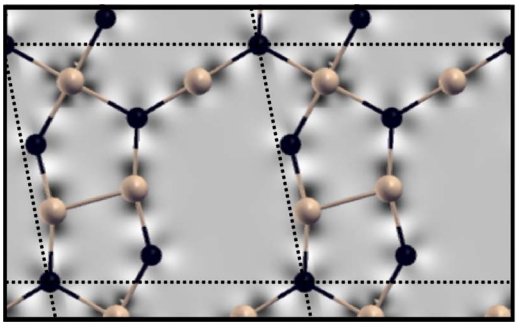

FIG. 5. (Color online) Charge density difference plot. The charge density difference between structure A and the superposition of atomic densities plotted in the plane of the structure; the scale runs from $-0.0005e$ (black) to $+0.0002e$ (white).

tailed understanding of bonding in the AuS layer. In Fig. 5, the charge density difference between structure A [Fig. 1(b)] and the superposition of atomic densities is plotted in the plane of the structure. From this plot, it is evident that charge accumulates between the Au and S atoms, apparently closer to the S. A small amount of charge accumulation appears between $Au_{(3,a)}$ and $Au_{(3,b)}$ as well. In order to gain additional chemical insight, we use a recently developed scheme[20] which provides a detailed description of bonding in well-characterized systems of both metallic and covalent nature. The analysis relies on the successive construction of two sets of localized Wannier orbitals with initially specified centers and symmetries (e.g., atomic s, p, or d symmetries). The first set (I) consists of atom-centered orbitals (AOs) and the second (II) of both AOs and bond-centered orbitals (BOs).

The construction of Wannier orbitals suited for the current application is described in detail in Ref. 20. Briefly, we make a choice of symmetry properties of Wannier functions specified with (a) the center of the Wannier function and (b) the irreducible representation of its site symmetry group given in terms of its partner function, for example, a spherical harmonic. Such a choice is typically guided by the symmetry properties of Bloch functions at high symmetry points in the Brillouin zone and is self-corrective, as discussed below. Well-localized Wannier functions can be obtained if they are Fourier transformed from Bloch functions that are smooth and periodic in the Bloch vector $\mathbf{k}$. As described in Ref. 20, these Bloch functions can in turn be obtained by introducing an auxiliary subspace constructed from highly localized functions of the chosen symmetry (a spherical harmonic for the angular part and a Gaussian for the radial part). These highly localized and orthonormal orbitals are Fourier transformed to obtain Bloch functions that span the auxiliary subspace. The key point is that these Bloch functions have the same symmetry properties as those of the Bloch functions in the physical subspace of occupied (and some of the unoccupied in metals) electronic states in the system. To obtain Bloch functions that are maximally smooth, a unitary transformation is performed on the Bloch functions in the physical subspace such that the overlap matrix between Bloch states of the auxiliary and the physical subspace becomes Hermitian (the rationale for this choice of unitary

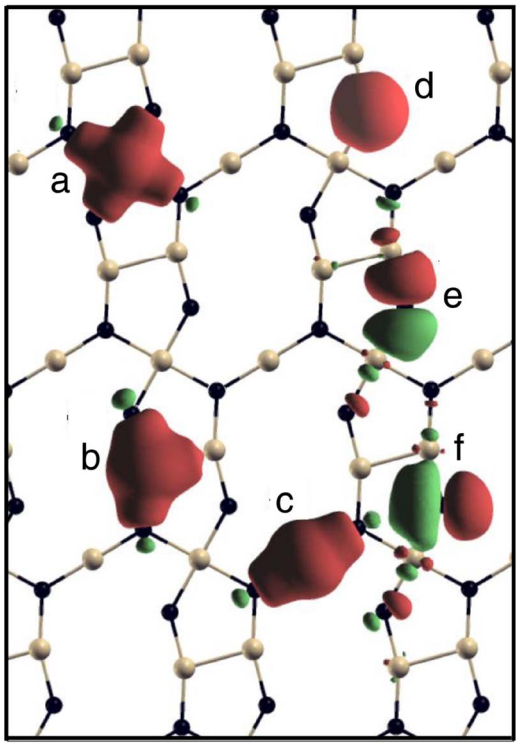

FIG. 6. (Color online) Atomic orbitals in structure *A*. 6*s* AOs for (a) $Au_{(4)}$, (b) $Au_{(3,a)}$ [similar to $Au_{(3,b)}$], and (c) $Au_{(2)}$; (d) 3*s* AOs; [(e) and (f)] 3*p* AOs for $S_{(2,b)}$ (similar to other S atoms). Red and green surfaces represent positive and negative contour surfaces of the same absolute value.

transformation is described in Ref. 20). This gives the desired Bloch functions and corresponding well-localized Wannier functions. Determination of the unitary transformation is facilitated by singular value decomposition of the overlap matrix. The scheme is self-corrective in the sense that some of the singular values vanish in the case where the choice of symmetry of the auxiliary subspace is not quite optimal and suggests that a different choice of symmetry should be made.

Another important feature of our approach[20] is that Bloch eigenfunctions are weighted by the square root of their occupation numbers in the above-described transformation. This allows treatment of metallic systems such as the ones considered here. Further, the resulting Wannier functions are no longer constrained to have unit charge as usual, but have an integrated charge that reflects the physics of the system. For example, the amount of charge in each localized AO and BO is directly related to atomic oxidation states and relative bond strengths, respectively.

VII. NATURE OF BONDING: RESULTS

We use here two choices of auxiliary subspaces: (I) one with only atom-centered orbitals (AOs) and (II) one with AOs and bond-centered orbitals (BOs) by including more unoccupied states in the physical subspace. We first illustrate the method by discussing results for the stable structure *A* [Fig. 1(b)]. The AOs for Au 6*s* [Figs. 6(a)–6(c)], S 3*s* [Fig. 6(d)], and S 3*p* [Figs. 6(e) and 6(f)] electrons are spatially extended, indicating that these electrons contribute substantially to bond covalency. In particular, the singular value for a Au-centered AO with *s* symmetry vanishes, reflected in the

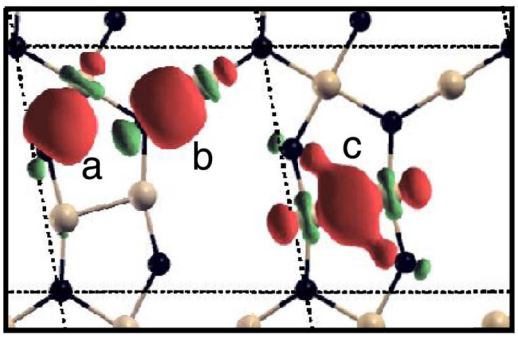

FIG. 7. (Color online) Bonding orbitals in structure *A*. (a) $Au_{(4)}$–S, (b) $Au_{(2)}$–S [similar to $Au_{(3,a)}$–S and $Au_{(3,b)}$–S], and (c) $Au_{(3,a)}$–$Au_{(3,b)}$. Symbols are the same as in Fig. 5.

distortion of these AOs from atomic-like *s* orbitals [Figs. 6(a)–6(c)], in contrast to the S AOs that still resemble atomic-like *s* and *p* orbitals [Figs. 6(e) and 6(f)]. This suggests an especially important role of Au 6*s* electrons in the covalency of bonds in the AuS layer. On the other hand, the Au 6*p* AOs are unoccupied and are especially localized, suggesting that the 6*p* orbitals of Au do not hybridize with 6*s* orbitals during bond formation. Au 5*d* AOs, although not spatially extended, are less localized than the 6*p* AOs and contribute to bond formation. This is consistent with the general argument in the literature that electronegative ligands of Au support Au 5*d* participation in bond formation, while electropositive ligands support Au 6*p* participation.[8] The electronegativity of S (Au) is 2.58 (2.54). The lack of 6*s*-6*p* hybridization is also consistent with the relatively large energy separation between 6*s* and 6*p* levels compared to 6*s* and 5*d* levels in atomic Au.[7]

The amount of electron charge in Au AOs is largest for $Au_{(2)}$ and smallest for $Au_{(4)}$, consistent with formal oxidation states expected from the literature. Au^{III} and Au^{I} have square planar and linear coordination geometries, respectively, while the $5d^9$ configuration in Au^{II} is typically accompanied by a Au–Au bond.[7] Indeed, the ring, $Au_{(4)}$–$S_{(3,b)}$–$Au_{(3,b)}$–$S_{(2,b)}$–$Au_{(4)}$–$S_{(3,a)}$–$Au_{(3,a)}$–$S_{(2,a)}$, is a motif found in Au^{2+} compounds.[7,17] S is known to form bonds with Au in all three oxidation states;[17] the two- and threefold coordinations for S are similar to those for O in Au_2O_3 (Ref. 21) (the structure of Au_2S_3 is unknown). The 1:1 stoichiometry in structure *A* thus arises from having one Au^{III} [$Au_{(4)}$], one Au^{I} [$Au_{(2)}$], and two Au^{II} [$Au_{(3,a)}$ and $Au_{(3,b)}$] atoms per unit cell, in contrast to bulk gold sulfides Au_2S and Au_2S_3,[15] which contain purely Au^{I} and Au^{III}, respectively.

Each Au (S) atom contributes $0.3e$–$0.4e$ ($0.8e$–$0.9e$) per bond. The Au–S bonds are partially polar, as indicated by their asymmetric BOs (Fig. 7). This is consistent with excess charge in S 3*p* AOs and depletion of charge in Au 6*s* (and some 5*d*) AOs. The origin of Au–Au interactions in Au^{II}–Au^{II} (and Au^{I}–Au^{I}) compounds has been the subject of debate.[8] Previous *ab initio* studies have described the Au^{II}–Au^{II} interaction as a single covalent bond with 6*s*-6*s* character.[8] Our calculations indicate that the 6*s* electrons indeed are key players in the Au–Au bond in the isolated AuS layer. We further predict that the Au–Au bond in isolated AuS is stabilized by delocalization over $S_{(2,a)}$ and $S_{(2,b)}$, as

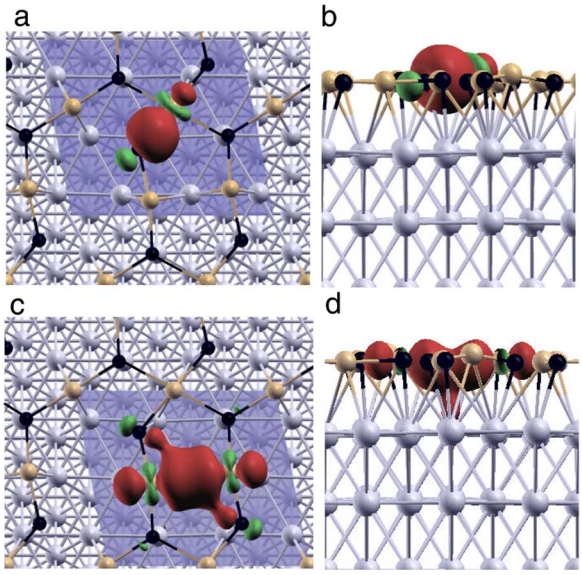

FIG. 8. (Color online) Bonding orbitals in structure *B*. $Au_{(2)}$–S in (a) top and (b) side views (similar for other Au–S bonds), and $Au_{(3,a)}$–$Au_{(3,b)}$ in (c) top and (d) side views. Symbols are the same as in Fig. 5. The isocontour value in (c) is half that in (a), (b), and (d).

indicated by the multicentered $Au_{(3,a)}$–$Au_{(3,b)}$ BO in Fig. 7(c). In addition, the amount of charge in the $Au_{(3,a)}$–$Au_{(3,b)}$ BO is 20%–27% less than that in the Au–S BOs, indicating that the Au–Au bond strength in isolated AuS is weaker than that of other bonds in the layer.

To understand the effects of the substrate, we performed a similar analysis on structure *B* [$Au_{(2)}$ at site × on Au(111) and $Au_{(4)}$ at ○ (Fig. 1)], with AOs centered on atoms in the AuS layer and the top Au(111) layer. The shapes of Au–S BOs are not affected by the substrate [Figs. 8(a) and 8(b)], while the multicentered Au–Au BO, though slightly extended towards the substrate atoms, remains largely confined within the AuS plane [Figs. 8(c) and 8(d)]. The fact that BOs within the AuS layer largely retain their shapes even in the presence of the Au(111) layers suggests that the AuS layer does not form strong directional bonds with the substrate, which is consistent with the experimentally observed incommensurability and our theoretical assumptions.

Compared to the isolated layer, the electronic charge in each BO increases by 54% on average, except for the Au–Au BO, where the increase is 15%. In contrast, the contribution of each AO to bonding either decreases or increases by at most 9%. This implies that bonds within the AuS layer are strengthened at the expense of substrate electrons and is consistent with our assumption that the AuS layer interacts with the substrate mainly through charge transfer. Using ΔE_F of 0.85 eV and the DOS of the isolated layer *A*, we estimate the quantity of charge transferred to the layer to be $\sim 3.3e$ per unit cell of *A*. Completely relaxing the isolated AuS layer in the presence of this extra charge does not change the atomic arrangements significantly [Fig. 2(b)]. The optimized lattice constants of the charged layer are 8.4 and 7.9 Å. These are near the low end but within the respective experimental ranges of 8.4–9.2 and 7.8–8.6 Å [see Table I for bond lengths]. The lattice angle of 76° is reasonably close to the experimental range of 78°–86°. These results are in contrast to what we found for the neutral AuS layer, where the optimized lattice constants were too small compared to experiment. This further confirms that charge transfer from the substrate stabilizes the stretched bonds in the supported layer, and that our estimated shift in E_F models the effect of charge transfer reasonably well.

The charge transfer described above, together with a reduction in surface energy of the otherwise exposed Au(111) surface, stabilizes the combined incommensurate system. The stabilization energy calculated for structure *B*, relative to the isolated AuS layer and the exposed Au(111) surface, is −4.32 eV/unit cell, or $-1.00\ \mathrm{J/m^2}$. In comparison, the Au surface energy is $1.62\ \mathrm{J/m^2}$.[22] On the other hand, the stabilization energy due to charging the isolated layer by $\sim 3.3e$ per unit cell is calculated to be −6.90 eV in a unit cell with 64 Å of vacuum between the AuS layers, or $-1.67\ \mathrm{J/m^2}$ (*k*-point sampling in the direction perpendicular to the layers verified that the AuS layers do not interact with one another in cells with half the vacuum height). Although the calculated charging energy may not be converged with respect to the vacuum height, it is clear that the energy of interaction between the layer and substrate arises from a reduction in surface energy and charge transfer, which strengthens the AuS intralayer bonds. In particular, the Wannier orbital analysis presented above shows that no strong directional bonds are present between the layer and substrate, so that the large interaction energy in structure *B* does not imply that the system prefers to be commensurate. The incommensurability is likely to arise from a mismatch between the experimental Au lattice and the optimum AuS lattice, taking into account charge transfer to the AuS layer.

VIII. CONCLUDING REMARKS

As previously established in detailed scanning probe studies,[5,6] the Au(111) surface interacts with deposited sulfur in a dynamic, rather than static, manner, eventually resulting in a 2D incommensurate Au–S phase upon annealing to 450 K. Experimental STM images alone cannot uniquely determine the atomic structure of the Au–S phase. In this work, we revisited the structure of this incommensurate phase and discussed in detail an atomic-scale model for the system, which agrees with high-magnification STM images. The proposed structure, derived for an isolated Au–S layer with stoichiometry of 1:1, is not affected by the presence of the Au substrate. The proposed structure reflects the rich coordination chemistry of Au, which is also present in Au compounds synthesized from Au ions in solution or gas phase.[7,8] We provide an interpretation of the stability of the model in terms of charge transfer from the substrate and the types of bonds and formal oxidation states of Au.

Our results do not constitute a proof for the thermodynamically stable structure; due to the many degrees of freedom in the system, a complete proof is beyond current computational capabilities. The exact orientation of the incommensurate layer on the substrate is also not completely understood. The insensitivity of the model to other effects, such as the substrate presence and charge transfer, suggests

that the proposed AuS structure may correspond to experimental observation or to a precursor state. Taken together with STM studies, our results imply that the Au(111) surface is not simply an "inert" surface, but can interact dynamically with deposited sulfur, with the incorporation of Au atoms from terrace sites into a sulfide adlayer at higher coverages. Our results also suggest that the ringlike features reported in the literature[14] may not simply be S_8 molecules. Similar adsorbate-induced mobilization of Au atoms has been observed when oxygen atoms are deposited onto Au(111), resulting in a gold oxide adlayer.[6]

The dynamic nature of the Au(111) surface and the incorporation of Au terrace atoms into a sulfide adlayer in this system have important implications for the structure of the S–Au interface in self-assembled monolayers of thiols on Au(111),[3] which is essential in determining their transport properties.[23] Etch pits and islands have also been observed in these systems, suggesting that Au terrace atoms will have similar interaction chemistry with thiol chains. The interface structure in thiol/Au systems has commonly been interpreted in terms of a flat Au(111) surface,[3] with only a few works[24] proposing an interface structure involving Au vacancies or adatoms. Recently, low temperature STM images[25] and x-ray standing wave experiments[26] have shown that alkanethiols bind to Au(111) through Au adatoms. These observations are consistent with the dynamic nature of Au(111) discussed in the present work.

ACKNOWLEDGMENTS

The authors acknowledge support from the Harvard NSEC, funded by NSF Grant No. DMR-02-13805. One of the authors (J.B.) acknowledges current support from U.S. DOE through the University of California, Lawrence Livermore National Laboratory. One of the authors (U.V.W.) acknowledges support from a DuPont Young Faculty grant. This work was partially supported by NCSA under DMR040002.

[1] G. Kresse, M. Schmid, E. Napetschnig, M. Shishkin, L. Kohler, and P. Varga, Science **308**, 1440 (2005).
[2] C. H. Ahn, K. M. Rabe, and J. M. Triscone, Science **303**, 488 (2004).
[3] J. C. Love, L. A. Estroff, J. K. Kriebel, R. G. Nuzzo, and G. M. Whitesides, Chem. Rev. (Washington, D.C.) **105**, 1103 (2005).
[4] C. T. Campbell, Surf. Sci. Rep. **27**, 1 (1997).
[5] M. M. Biener, J. Biener, and C. M. Friend, Langmuir **21**, 1668 (2005).
[6] B. K. Min, A. R. Alemozafar, M. M. Biener, J. Biener, and C. M. Friend, Top. Catal. **36**, 77 (2005).
[7] R. J. Puddephatt, *The Chemistry of Gold* (Elsevier, New York, 1978).
[8] P. Pyykko, Angew. Chem., Int. Ed. **43**, 4412 (2004).
[9] M. M. Biener, J. Biener, and C. M. Friend, Surf. Sci. **590**, L259 (2005).
[10] J. P. Perdew and Y. Wang, Phys. Rev. B **45**, 13244 (1992).
[11] P. E. Blochl, Phys. Rev. B **50**, 17953 (1994).
[12] E. Lundgren, G. Kresse, C. Klein, M. Borg, J. N. Andersen, M. De Santis, Y. Gauthier, C. Konvicka, M. Schmid, and P. Varga, Phys. Rev. Lett. **88**, 246103 (2002).
[13] T. Wiederholt, H. Brune, J. Wintterlin, R. J. Behm, and G. Ertl, Surf. Sci. **324**, 91 (1995).
[14] X. P. Gao, Y. Zhang, and M. J. Weaver, J. Phys. Chem. **96**, 4156 (1992); C. Vericat, G. Andreasen, M. E. Vela, and R. C. Salvarezza, J. Phys. Chem. B **104**, 302 (2000); C. Vericat, M. E. Vela, G. Andreasen, R. C. Salvarezza, L. Vazquez, and J. A. Martin-Gago, Langmuir **17**, 4919 (2001); C. Vericat, M. E. Vela, G. A. Andreasen, R. C. Salvarezza, F. Borgatti, R. Felici, T. L. Lee, F. Renner, J. Zegenhagen, and J. A. Martin-Gago, Phys. Rev. Lett. **90**, 075506 (2003).
[15] J. C. Bailar, H. J. Emeleus, R. Nyholm, and A. F. Trotman-Dickenson, *Comprehensive Inorganic Chemistry* (Pergamon, New York, 1973).
[16] K. Ishikawa, T. Isonaga, S. Wakita, and Y. Suzuki, Solid State Ionics **79**, 60 (1995).
[17] H. Schmidbaur, *Gold: Progress in Chemistry, Biochemistry and Technology* (Wiley, New York, 1999).
[18] S. Hufner, *Photoelectron Spectroscopy: Principles and Applications*, 3rd ed. (Springer-Verlag, Berlin, 2003).
[19] J. Tersoff and D. R. Hamann, Phys. Rev. Lett. **50**, 1998 (1983).
[20] J. Bhattacharjee and U. V. Waghmare, Phys. Rev. B **73**, 121102(R) (2006).
[21] P. G. Jones, H. Rumpel, E. Schwarzmann, G. M. Sheldrick, and H. Paulus, Acta Crystallogr., Sect. B: Struct. Crystallogr. Cryst. Chem. **35**, 1435 (1979).
[22] L. Z. Mezey and J. Giber, Jpn. J. Appl. Phys., Part 1 **21**, 1569 (1982).
[23] G. K. Ramachandran, T. J. Hopson, A. M. Rawlett, L. A. Nagahara, A. Primak, and S. M. Lindsay, Science **300**, 1413 (2003); E. G. Emberly and G. Kirczenow, Phys. Rev. Lett. **91**, 188301 (2003); Z. Hens, D. V. Tallapin, H. Weller, and D. Vanmaekelbergh, Appl. Phys. Lett. **81**, 4245 (2002).
[24] L. M. Molina and B. Hammer, Chem. Phys. Lett. **360**, 264 (2002); Y. Morikawa, C. C. Liew, and H. Nozoye, Surf. Sci. **514**, 389 (2002).
[25] P. Maksymovych, D. C. Sorescu, and J. T. Yates, Jr., Phys. Rev. Lett. **97**, 146103 (2006).
[26] M. Yu, N. Bovet, C. J. Satterley, S. Bengio, K. R. J. Lovelock, P. K. Milligan, R. G. Jones, D. P. Woodruff, and V. Dhanak, Phys. Rev. Lett. **97**, 166102 (2006).